

Reports

Bistatic-Radar Observation of Long-Period, Directional Ocean-Wave Spectra with Loran A

Abstract. Bistatic-radar scattering from medium- to long-wavelength (80 to 200 meters) ocean waves has been observed with the use of loran A (1.85 megahertz) transmissions and a receiver located 280 kilometers away. The received echoes have been converted into a time-delay, Doppler-frequency map in which the effects of anisotropies in the ocean-wave spectra are clearly shown. The distribution of the echoes in delay-Doppler space is consistent with Bragg scattering from trains of dispersed ocean waves.

Bragg (or resonant) scattering from ocean-wave structures has been proposed by Crombie as a principal source of medium- to long-wavelength (15 to 300 m) radar echoes from the surface of the sea (1). A small body of experimental and theoretical literature (2), dealing mostly with backscatter effects in this frequency range, provides some credible evidence for the Bragg scattering mechanism, but relatively little systematic investigation of the scattering process has been carried out.

Peterson, Munk, and Nierenberg, on the assumption that the Bragg hypothesis is correct, have recently proposed a bistatic-radar method for determining the directional wave spectra of the sea (3). In this report we briefly describe the proposed technique and present new observational results from an experiment to determine its feasibility. We believe our experimental results strongly support the Bragg mechanism as the principal source of long-wavelength radar echoes from the sea. In addition, the effects of anisotropies in the ocean-wave spectra are clearly present. One earlier experiment (4) is known in which bistatic geometry and loran A transmissions were used, but this experiment differs from the work reported here in the methods of data processing, analysis, and interpretation.

Briefly, the Bragg scattering hypothesis is as follows. The ocean surface at any particular point is considered to be made up of linearly superposed gravity wave components, each of which travels in a particular direction with a phase velocity v given by $v^2 = gL/2\pi$, where g is the acceleration due to gravity and L is the wavelength. Strong

radar echoes are obtained only from those particular components of the wave spectrum that satisfy the condition for resonant scattering from periodic structures. If we assume that waves propagate along the surface, this condition is that the distance L between wave crests is given by

$$L = (n\lambda \sec \eta/2)/2$$

where λ is the wavelength of the incident probing wave, $\eta/2$ is the half-angle between the radar transmitter and the receiver at the scattering point, and n is an integer greater than zero. Other nonresonant scattering mechanisms un-

doubtedly exist but are believed to play only a minor role in this wavelength regime. Since the Bragg condition is satisfied only by those wave components whose perpendiculars bisect the angle included between the transmitter and the receiver, it is selective in terms of the direction of travel and ocean wavelength from which echoes are obtained.

In our experiments we used coherent pulse trains from two loran A stations at Point Arena and Point Arguello on the California coast. The receiver was located almost midway between the two transmitters at Sunset Beach. The pulses were of approximately gaussian shape, had a duration of 50 μ sec, and were repeated at 29.8-msec intervals. Although signals were always received from both stations, the differences in their arrival times allowed them to be separated and treated independently in the data processing. Because of the very long radio wavelength of the loran A transmitter with respect to observed ocean-wave spectra, it was assumed that the Bragg condition would be fulfilled only for the first-order resonance, $n = 1$. Furthermore, on theoretical grounds, echoes corresponding to $n > 1$ are expected to be relatively much weaker. These assumptions were later borne out by the data. A map of the California coast (Fig. 1) shows the geometry of the experiment.

The unique features of the experiment reported here arise from the combination of the bistatic geometry and the Bragg scattering mechanism. According to elementary geometrical principles, the locus of all scattering points that form echoes with the same time-delay excess (after the arrival of the direct wave) is an ellipse with foci at the transmitting and receiving sites. The line perpendicular to an ellipse at any point is also the bisector of the angle subtended by the lines between the foci and that point. Consequently, to satisfy the Bragg hypothesis, a particular ocean-wave component must be propagating along a line perpendicular to the ellipse on which it is observed, and it must have the proper spatial period. As a consequence of the secant $\eta/2$ law, the longest observable ocean waves move along the semiminor axis of the ellipse, whereas the shortest waves travel along an extension of the line connecting the transmitter and the receiver.

Echoes from the sea are also shifted in frequency by the motion of the waves. It is a simple matter to show that, owing to the dispersive nature of

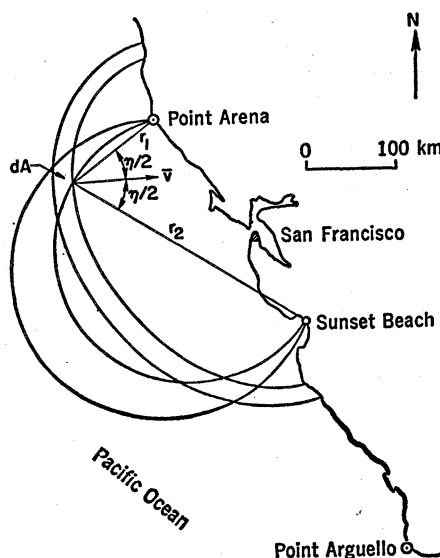


Fig. 1. Bistatic-radar geometry. Loran A transmitters are located on the California coast at Point Arena and Point Arguello; the receiving site is at Sunset Beach. The geometrical figures are ellipses, with foci at Point Arena and Sunset Beach, and circles which contain the line between Point Arena and Sunset Beach as a chord.

the gravity waves, each wavelength observed at a fixed time delay has a unique Doppler shift. Thus, a simultaneous determination of time-delay and Doppler shift permits resolution of the echo into a spectrum which can be associated with a unique set of ocean-wave components.

The loci of points of constant Doppler shift may also be given a simple geometrical interpretation. Constant Doppler shifts arise from those points where the transmitter-receiver base line subtends a constant angle. All such points lie on a circle which contains the base line as a chord. Unfortunately, the orientation of the waves has no particular relation to the circle, as it does to the ellipse. A pair of ellipses and circles, representing the delay and Doppler loci, have been superposed on Fig. 1.

Using the dispersion relationship and the Bragg condition given above, one can show that

$$f_{\text{Doppler}} = \pm \sqrt{(g/\pi\lambda) \cos \eta/2} = \pm f_{\text{max}} \sqrt{\cos \eta/2}$$

is the equation for the Doppler shift of the radar echo. It may also be shown that the Doppler shift is exactly equal to the ocean-wave frequency.

The receiver output is processed by the use of standard delay-Doppler techniques. Successive data samples, taken at a fixed time-delay excess after the arrival of the direct pulse, are formed into estimates of power spectral density as a function of delay. These estimates are then displayed on delay-Doppler coordinates in the usual manner (5). To the first order, the echoes are sorted into a set of mutual delay-Doppler bins of dimensions comparable to the transmitter pulse length and the reciprocal of the observation time, respectively. However, the amplitude effects associated with variations in the propagation path lengths and the areal extent of the echoing area must be accounted for. It is clear from Fig. 1 that the surface area contained within the intersection of two successive delay and Doppler loci is not constant. Furthermore, the propagation path loss, which is inversely proportional to the square of the product of the distances to and from the echoing point, r_1 and r_2 , respectively, also varies with location on the ocean surface. These areal and propagation effects may be expressed in terms of the delay-Doppler coordinates as

$$\frac{dA}{r_1^2 r_2^2} = \left| \frac{8}{a^2 (\xi^2 - 1)} \times \frac{\alpha^8}{\{(1 - \alpha^4) [1 - \xi^2 (1 - \alpha^4)]\}^{\frac{3}{2}}} d\alpha d\xi \right|$$

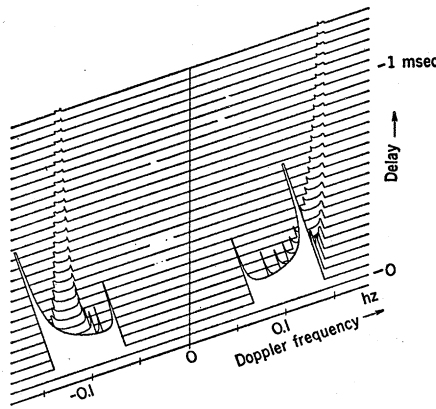


Fig. 2. Predicted delay-Doppler spectrum from a homogeneous, isotropic sea. It is assumed that the radar cross section per unit surface area is independent of wavelength. The spectrum for zero delay is not shown.

where a is the distance between the transmitter and the receiver, $\alpha = f_{\text{Doppler}}/f_{\text{max}}$ and $\xi = (r_1 + r_2)/a$ are the normalized delay-Doppler coordinates of the echo, and dA is the differential element of the surface area contained in $(\alpha, \alpha + d\alpha)$ and $(\xi, \xi + d\xi)$.

The amplitude weighting function, given above, is plotted in Fig. 2, with an arbitrary ordinate scale. Since no directional or wavelength dependencies in the ocean-wave spectrum are included, this plot may also be interpreted as the echo delay spectrum expected from a homogeneous, isotropic, uniformly scattering sea. Echoes may be observed only within a certain permitted region of the delay-Doppler space. The sharp cutoffs in delay-Doppler coordinates arise jointly from the Bragg scattering assumptions and the dispersion relation for gravity waves. Echoes from near the experiment base line are weighted most heavily. Echo strength decays slowly with increasing delay because the propagation losses are partially compensated by a very rapidly increasing element of area. The observed delay-Doppler spectra will be somewhat smoother than the one shown here because of the averaging effects of finite pulse widths and frequency windows.

A geometric analysis of the point mapping from ocean-wave spectrum space to delay-Doppler space has been carried out by Nierenberg and Munk (6). Barrick has examined the details of the scattering process, using perturbation theory under the assumption of a gently undulating sea (7).

The loran A transmitters at Point Arena and Point Arguello operate on a carrier frequency of 1.85 Mhz or

162-m wavelength with a peak transmitted power in excess of 800 kw (8). The transmitted frequency is derived from an oscillator having a stability of one part in 10^9 or better. The spectra of the direct signals from two of the stations were examined at high resolution and were found to be less than 0.002 hz in width at the -20 db points. Echoes with signal-to-noise ratios of 10 to 20 db are obtained. A number of different stations operate on the same frequency, but these stations may be distinguished by their repetition rates, or, in the case of pairs of stations for which the same repetition rate is used, by the time phase of the pulse transmissions.

Observations were made in the late afternoon of 15 March 1970. Signals with the common pulse period of 29.8 msec from Point Arena and Point Arguello were used. Spurious signals from other loran transmissions on the same frequency were present, but we have eliminated these from the data by taking advantage of their known periodicities.

A coherent detection scheme with a single radio-frequency mixer was used to receive the echoes. Spectral estimates with a resolution of 0.003 hz were formed from sets of samples taken at the same excess delay, corresponding to a path length difference of 15 km, with the use of a Hamming data window and a single Fourier transform. The coherence properties of the sea surface are not yet sufficiently well understood to permit a calculation of the reliability of the spectral estimates.

The delay-Doppler transforms of the signals from Point Arena and Point Arguello are shown in Fig. 3. Successive range bins are presented in isometric projection. Positive Doppler shifts are to the right and correspond to waves approaching the transmitter-receiver base line. The large, narrow spike in the center of each part of Fig. 3 is the direct, unshifted signal, followed by reflections from stationary objects. The theoretically predicted maximum and minimum Doppler shifts, under the Bragg scattering assumption, are indicated by the solid lines. Data from the two stations were taken about an hour apart, so they do not represent simultaneous measurements. However, the sea conditions should not have changed appreciably during the period of the two measurements. The ordinate is linear in power. However, the scales, which are arbitrary, differ by a factor of 5; the data from Point Arena are

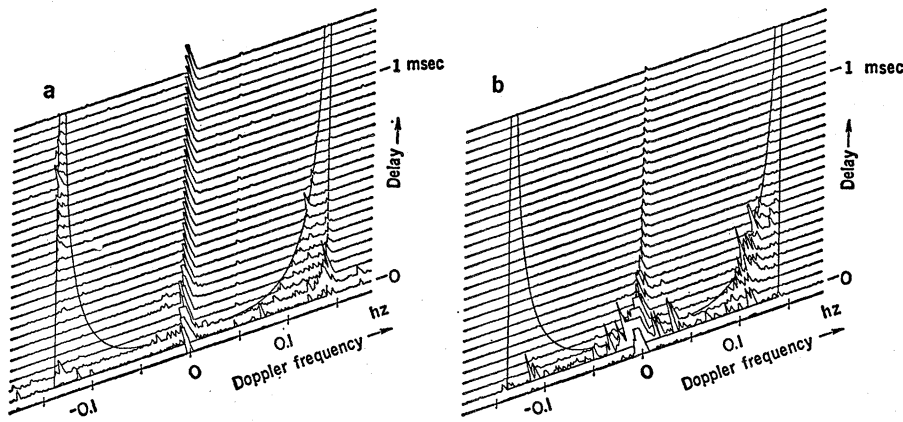


Fig. 3. Observed delay-Doppler spectra from (a) Point Arena to Sunset Beach and (b) Point Arguello to Sunset Beach stations, 15 March 1970. Solid lines indicate the boundaries of echoes under a Bragg scattering hypothesis. Each delay increment represents an increase of 15 km in the propagation path length.

exaggerated with respect to those from Point Arguello.

Several features of the data are worth noting. First, the Doppler-shifted sea echoes closely follow the range of frequencies predicted by the Bragg-scattering mechanism and gravity wave propagation. Second, almost all of the echoes from Point Arguello, and the echoes from Point Arena in the first several range bins, represent waves whose motion was predominantly toward the coastline. Those echoes from Point Arena in later range bins represent waves moving away from the coastline. There is a region in the Point Arena data, between delays of 300 to 600 μsec , where there are waves traveling both toward and away from the coastline. These waves may have coexisted in the form of standing waves, or may have been in quite separate parts of the sea as mirror images about the perpendicular bisector of the experiment base line. At delays greater than 600 μsec there are strong echoes from waves moving away from the coast. No waves moving toward the coast were observed at long delays.

It appears that the strongest reflections originated in a region between Sunset Beach and Point Arguello, extending from about 50 to 125 km from the shore. These echoes originate in an area where the ambiguities of interpretation are minimal and correspond to waves traveling toward the shore. In the Point Arena data, strong reflections could have arisen in patches of ocean within about 20 km of either Sunset Beach or Point Arena with the waves traveling toward the shore, and in regions 70 to 140 km offshore, again from either Sunset Beach or Point Arena,

with waves traveling away from the shore. In future experiments antenna directivity may be used to resolve the ambiguities. However, on the basis of the prevailing wave patterns near the coast, it appears likely that the near-coastal echoes came from an area near Point Arena. Echoes corresponding to n greater than unity in the Bragg equation would have Doppler shifts that vary as \sqrt{n} . No such echoes were observed.

We interpret the predominant features in the observed scattering function as being due to Bragg scattering from extremely long-period components of the ocean-wave spectrum, principally on the basis of the strict conformity of the delay-Doppler spectra to that predicted by the Bragg scattering hypothesis. For the most part, no distinct echoes appear outside the permitted region, whereas for those regions where echoes are present in great density the echoes follow the limits of the Bragg scattering curve within the resolution of the experiment. One major exception to this general statement occurs in the data from Point Arena at short delays, that is, from areas closest to the California coast. Here there is a Doppler shift slightly greater than that predicted by the Bragg mechanism, corresponding to motion along the experiment base line of about 1 foot (0.30 m) per second. We believe that this discrepancy is due to current flowing parallel to the coast (southeast) in this area. Such a current movement would be expected to offset the entire delay-Doppler spectrum in frequency by an amount corresponding to the component of the current velocity normal to the echoing wave. We are unable to explain

the several additional small echoes that appear in the data.

This experiment has demonstrated the possibility for remote sensing of directional ocean-wave spectra by the bistatic observation of Bragg scattering of radio waves. Time-delay, Doppler-shift processing of the scattered radio signals provides areal resolution and the identification of ocean waves of particular lengths and their direction of travel. The ocean waves described in this report have lengths of between 81 and about 200 m, probably "swell" from distant sources.

The theory of ocean wave generation suggests that wavelengths with speeds up to the surface wind speed are excited when sufficient fetch exists. A long-wavelength cutoff is predicted since longer waves would travel faster than the winds that generate them (9). Observations in which multiple frequencies are used should permit the measurement of this cutoff wavelength and hence give information on surface wind speeds in the generation region.

More refined, multifrequency experiments could make possible the measurement of the power spectral density of the ocean surface over a range of surface scales. Two-dimensional ocean-wave spectra could be obtained from bistatic multifrequency observations similar to the single-frequency measurements described in this report. Alternatively, highly directional antennas might be used with monostatic multifrequency radars. Surface wave propagation should permit observations at distances of up to about 500 km from the observing stations. Very much larger regions should be observable if ionospherically propagated transmissions were used. In this case, however, great care would be required to correct the observations for Doppler shifts caused by variation with time of reflection height from the ionosphere. These shifts could be greater than the Doppler shifts produced by ocean waves. In addition, more than one propagation mode may be present simultaneously with differing Doppler shifts. Ionospheric absorption would limit low-frequency observations during the daytime, whereas high-frequency propagation would be limited during the night by reduced ionospheric electron density. It appears probable that it would be possible to observe the cutoff wavelength of ocean spectra with the use of ionospheric propagation. However, variations of propagation loss

with frequency would probably limit the accurate measurement of ocean-wave spectra if ionospheric propagation were used.

ALLEN M. PETERSON
CALVIN C. TEAGUE
G. LEONARD TYLER

Center for Radar Astronomy,
Stanford University,
Stanford, California 94305

References and Notes

1. D. D. Crombie, *Nature* **175**, 681 (1955).
2. ——— and J. M. Watts, *Deep-Sea Res.* **15**, 81 (1968); J. G. Steele, *Aust. J. Phys.* **18**, 317 (1965); L. H. Tveten, *Science* **157**, 1302 (1967).
3. A. M. Peterson, W. H. Munk, and W. A. Nierenberg specifically discussed this type of

- experiment at Scripps Oceanographic Institute, La Jolla, Calif., July 1968, during a Jason summer study program. We have also discussed the experiment with D. D. Crombie and D. E. Barrick.
4. E. P. Anderson, thesis, Stanford University (1957).
 5. J. V. Evans and T. Hagfors, *Radar Astronomy* (McGraw-Hill, New York, 1968).
 6. W. A. Nierenberg and W. H. Munk, Jason working paper, Scripps Oceanographic Institute, La Jolla, Calif., 1969.
 7. D. E. Barrick, *Advan. Res. Projects Agency Order No. 1178* (Battelle Memorial Institute, Columbus, Ohio, 1970).
 8. *Radio Aids to Maritime Navigation and Hydrography* (International Hydrographic Bureau, Monte Carlo, Monaco, 1965).
 9. W. H. Munk and W. A. Nierenberg, *Nature* **224**, 1285 (1969).
 10. Supported in part by NASA grant NGL 05-020-014. We thank D. H. H. Ingalls and B. Warsavage for their help in preparing the computer programs.

1 June 1970; revised 29 July 1970

Potassium-Argon Ages of Lunar Rocks from Mare Tranquillitatis and Oceanus Procellarum

Abstract. *Crystalline rocks from Mare Tranquillitatis have yielded potassium-argon dates as old as 3.8×10^9 years. Crystalline rocks from Oceanus Procellarum give potassium-argon ages as old as 2.8×10^9 years. Evidently the maria are ancient features of the moon and were not formed contemporaneously, a conclusion that also has been verified by other methods. The potassium-argon ages of rocks from Oceanus Procellarum show much more loss of argon than the rocks from Mare Tranquillitatis, an indication that the rocks at Oceanus Procellarum have experienced more severe shock effects or longer cooling rates.*

Analyses of argon in the Apollo 11 crystalline rocks returned from Mare Tranquillitatis were performed in the National Aeronautics and Space Administration Lunar Receiving Laboratory. When these determinations are combined with the best available potassium values, in many cases from adjacent samples (1, 2), these rocks give K-Ar ages in the range of 2.2 to 3.8×10^9 years.

We have recently determined K-Ar ages of 21 whole rock samples returned by Apollo 12 from Oceanus Procellarum. These ages are the first of this type to be obtained on Apollo 12 material. We measured the argon content by mass spectrometry, using the basic techniques described previously (1, 3). The potassium content, in most cases in adjacent samples, was determined by optical emission and atomic adsorption spectroscopy (3, 4). The potassium content for rock 12054 was obtained by gamma-ray analysis and that for rock 12055 was obtained from the average of Apollo 12 crystalline rocks (3).

A histogram of K-Ar ages for 20 Apollo 12 rocks is shown in Fig. 1. The precision of the analytical results is such that the error of the K-Ar ages is less than 0.1×10^9 years. For comparison,

the histogram of Apollo 11 rocks is also given (5, 6). The Apollo 12 samples show a range in K-Ar ages of 1.4 to 2.8×10^9 years.

An exceptional Apollo 12 rock not shown on the histogram of Fig. 1 is sample 12013. This rock is very different from other lunar rocks of both Apollo 11 and Apollo 12 in both its chemistry and noble gas content (3). It appears to be an igneous or volcanic breccia containing about 70 percent anorthitic plagioclase. It is enriched in

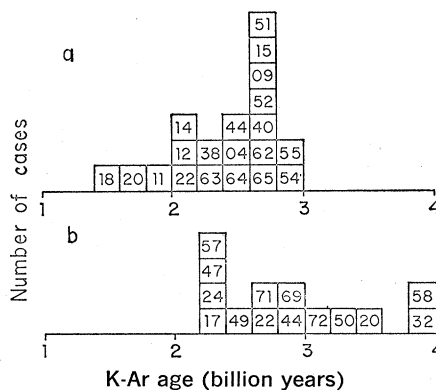


Fig. 1. Histogram of K-Ar ages of lunar rocks. (a) Apollo 12; (b) Apollo 11. The numbers in each block refer to the last two digits of the generic sample number.

K and U and is similar to the residual melt of a fractional crystallization (3). Table 1 presents a summary of the crystallization ages of K, U, He, and Ar determined in rock 12013. Three measurements were made for one single chip. The sample for measurement 1 was a single piece, for measurement 2 a crushed piece, and for measurement 3 a finely ground portion. The concentrations of radiogenic argon and helium are very large, as would be expected from the high potassium and uranium contents. It is apparent from the data in Table 1 that the concentrations of radiogenic ^4He and spallogenic ^3He and ^{36}Ar (also ^{21}Ne and ^{38}Ar) are essentially the same for the three measurements of rock 12013. However, the concentration of radiogenic ^{40}Ar in measurement 1, the uncrushed piece, is an order of magnitude greater than that in the crushed samples (measurements 2 and 3). The K-Ar age drops from the high value of 7.9×10^9 years for the uncrushed piece to between 3.6 and 3.8×10^9 years for the crushed sample. This sample apparently contained excess radiogenic argon in voids so that simple crushing released it. The loss of this excess ^{40}Ar must have been essentially complete for after continued grinding of the rock (measurement 3) there was no further reduction in the ^{40}Ar content. That no ^{40}Ar produced in situ was released during crushing can be inferred from the constant concentration of ^4He for all three measurements. The U-He age is only 1.4×10^9 years, far lower than the K-Ar age. This indicates that a portion of the ^{40}Ar produced in situ may have been lost with the ^4He sometime during the rock's history. Thus, the K-Ar ages of measurements 2 and 3 (which are in agreement within the limits of our experimental and sampling errors) may represent a lower limit to the age of crystallization of rock 12013. This age is much greater than any K-Ar age listed in Fig. 1 for other Apollo 12 rocks.

Rock 12013 seems to represent very old material and was ejected to the Apollo 12 landing site a relatively short time ago. The surface exposure age is about 35 million years (7). The Xe content consists mainly of a trapped component with about 10 percent spallogenic Xe. There is, however, less than 10^{-11} cm³/g of excess ^{129}Xe from the decay of extinct ^{129}I (as well as fissionogenic xenon from plutonium), as compared with the xenon component trapped in the solar wind (8) and with